Experimental and Numerical Study of a Transient, Two-Dimensional Unsaturated-Saturated Water Table Recharge Problem

M. VAUCLIN

Institut de Mécanique de Grenoble, Université Scientifique et Médicale, 38041 Grenoble-Cédex, France

D. KHANJI

Department of Civil Engineering, University of Aleppo, Aleppo, Arab Republic of Syria

G. VACHAUD

Institut de Mécanique de Grenoble, Université Scientifique et Médicale, 38041 Grenoble-Cédex, France

Transient two-dimensional water flow is studied in relation to the recharge of a water table aquifer. The approach is based on the physics of water transfer in the complete domain defined by both the saturated and unsaturated zones of soil. Experimental data were first obtained in a slab of soil (3 m in length, 2 m in height, and 5 cm in thickness) in which the changes of water content and water pressure occurring in the flow domain were measured throughout an artificial recharge event. These were compared with the predictions of a numerical model based on the continuity of transfer between the unsaturated and saturated zones. The validity of the model is proved by the excellent agreement between simulated and experimental results. Furthermore, comparison with the results obtained by a viscous flow analog reveals the errors associated with the traditional free surface approach, which neglects transfer in the unsaturated zone.

Because of the increasing demand for water to supply urban areas, the ability to predict the rate of recharge of free surface aquifers in both artificial conditions (e.g., irrigation, furrow) and in nature (e.g., ponds, rainfall) has become of prime importance. Not only is quantity important but also quality because pollution due to contaminants in the soil frequently occurs. Quality has become crucial in many areas because of the extensive use of landfills for waste disposal.

This paper is concerned with the development of a numerical model for predicting the response of a shallow water table to infiltration from the soil surface taking into account the transfer of water in the unsaturated zone. A transient, isothermal, two-dimensional flow system in an incompressible material is considered. The air phase is assumed to be at atmospheric pressure. The equation used is for a unified model of saturated-unsaturated flow.

Compared to other papers with a unified treatment of unsaturated flow [*Rubin*, 1968; *Freeze*, 1971; *Cooley*, 1971; *Narasimham*, 1975], the present approach is original because the numerical simulation is tested on a series of experimental data obtained in a two-dimensional sand box. Very recently, *Narasimhan and Witherspoon* [1978] have also presented a mixed explicit-implicit scheme for solving the Richard's equation which has been tested on a drainage experiment [*Vauclin*, 1975] performed in the same sand box. Their numerical results are in good agreement with experimental data and with the results obtained by the model described in this paper.

In the first part of this work, the experimental method is presented, while in the second part the numerical analysis of the problem using a finite difference scheme is described.

EXPERIMENTAL METHOD

Definition of the Problem

Figure 1*a* presents a schematic diagram of the flow domain to be considered. It consists of a slab of homogeneous soil underlain by horizontal barrier located at depth P from the soil surface and divided by equally spaced trenches with spacing $2L$. The trenches are assumed to penetrate the soil to the bottom, with a horizontal water table located at depth H_0. Water is supplied at a constant rate q_0 from a series of infinite lines of finite width $2L_0$ centered between the trenches. The water level in the trenches is maintained constant at the depth H_0, by a drainage system.

Because of symmetry, only the cross-hatched section on Figure 1*a* need be considered. The origin 0 is at the upper left hand corner of the slab; x is oriented to the right, and z is vertically downward. Flow is assumed to be planar.

Flow Domain and Its Experimental Simulation

Experiments were run in the laboratory on a slab of soil 3 m long, 2 m high, and 5 cm thick which corresponds to the cross-hatched domain in Figure 1*a*. The soil was packed as homogeneously as possible (with an average dry density of 1.57 g/cm^3) between two perspex walls supported by a frame resting on an impervious horizontal boundary. One of the vertical ends of the slab was connected to a constant head reservoir used both to set the height of the piezometric level and to measure directly the total volumetric outflow from the slab (Figure 1*b*).

The soil used as the porous medium was a fine river sand of fairly regular grain-size distribution, 50% in weight passing through a mesh of 0.3 mm. The granulometric curve is shown on Figure 2*a*.

A water table was imposed at the depth $H_0 = 135$ cm, but the experiments were begun only when hydrostatic equilibrium had been obtained throughout the flow domain.

For the particular case defined by Figure 1*b*, the boundary conditions applied on this slab were

Vertical left hand side (OA in Figure 1b). By symmetry this is a flow line. Consequently, there is no flow through the side.

Vertical right hand side (CB in Figure 1b). The water level

Paper number 9W0657.
0043-1397/79/009W-0657$01.00

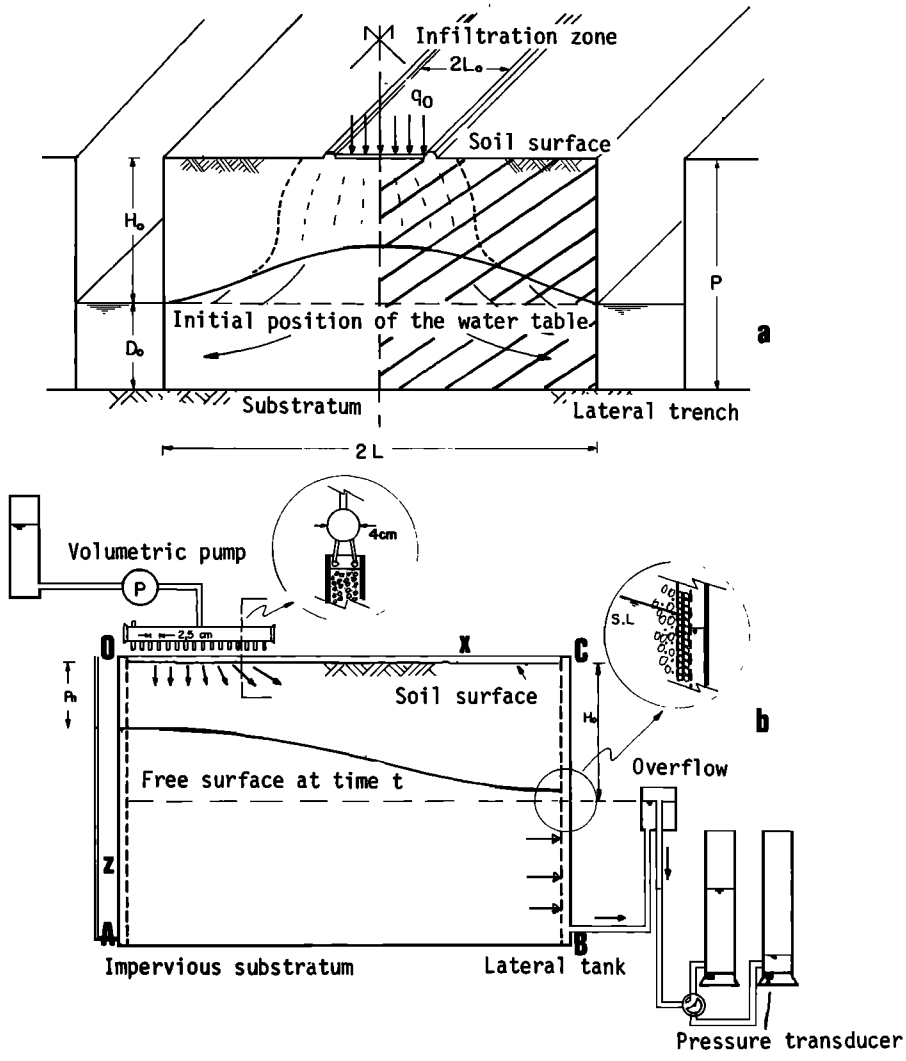

Fig. 1. (*a*) Schematic diagram of the flow domain. (*b*) Experimental details.

remains constant in the ditch. The constant head reservoir is maintained at depth H_0, and overflow from the reservoir is recorded.

Soil surface (OC). A constant flux corresponding to q_0 = 14.8 cm/hr is applied over a width L_0 = 50 cm. The constant flow device consists of thick wall rubber cylinder, 4 cm in diameter, 50 cm long, equipped with a series of hypodermic needles (about 80) and connected to a volumetric pump. This system allows a precisely reproducible and constant flux to be obtained throughout the entire length of the tubing for the duration of the experiment. The value of q_0 is chosen to be smaller than the saturated hydraulic conductivity of this material (K_s = 35 cm/hr). The remaining soil surface is covered in order to prevent evaporation. Water was supplied for 8 hr, the water table beginning to rise after 1.75 hr.

Bottom of the slab (AB). This is an impervious, horizontal substratum.

During the infiltration, the following measurements were made: (1) changes of volumetric water content θ in cm³/cm³ and water pressure head h in cm of water for the whole flow domain, (2) rate of advance of the wetting front, (3) outflow volume, and (4) position of free water table at $x = 0$ and $x = L$.

Measurement Techniques

The experimental methods for measurement of $\theta(x, z, t)$ and of $h(x, z, t)$ have been described in some detail previously [*Vachaud et al.*, 1973]. In brief, water content θ is obtained from the attenuation of gamma rays emitted by a source of Am 241. To provide enough measurement points, three sources of gamma rays are used simultaneously, a monitoring technique, analogous to the one developed by *Vachaud and Thony* [1971], being adapted to this problem. It is based on the use of two measurement platforms, one for the sources, the other for the detectors. Each platform is equipped with three sensors: two on the same horizontal line, 30 cm apart, two on the same vertical line, 20 cm apart. Each detector is connected to its own scaler. It is thus possible, for a given position of the platform in the x-z plane, simultaneously and independently to measure changes of water content at three points. Automatic displacement of the platforms in the horizontal or in the vertical is controlled, at the end of a counting sequence, by two independent motors. The displacements are accomplished in such a way that the platforms can be returned consistently to the same positions.

The standard procedure used is to measure the water con-

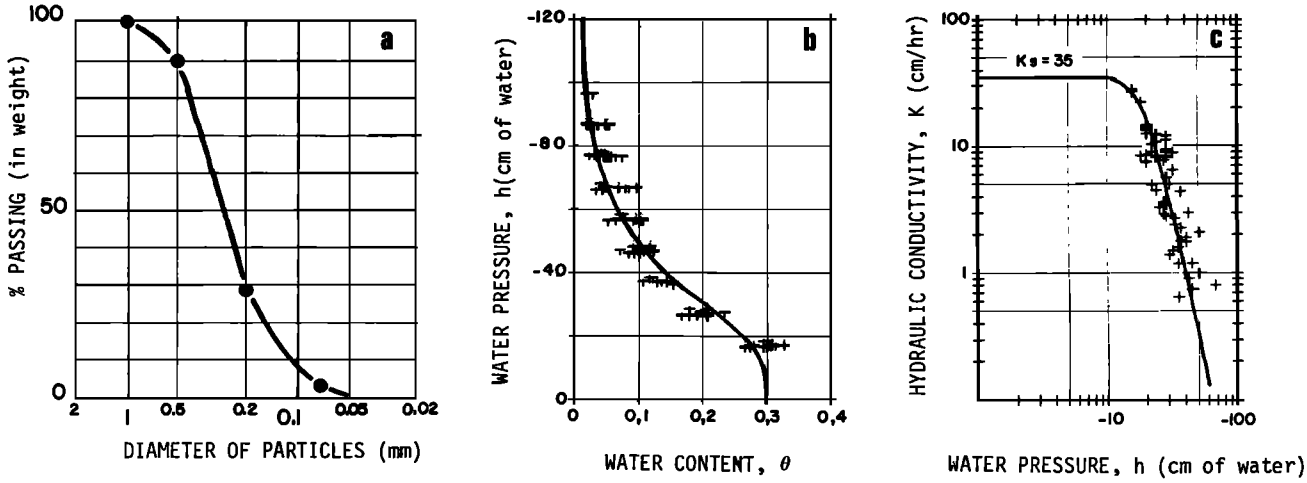

Fig. 2. Soil properties. (*a*) Granulometric curve. (*b*) Suction curve. (*c*) Hydraulic conductivity curve.

tent at points in a grid formed by a matrix in the x-z plane, with spacings $\Delta z = 10$ cm and $\Delta x = 30$ cm starting from $x = 20$ and $z = 10$ cm. During infiltration the domain of measurements is confined to the wetting zone, which is very clearly determined by visual observation of the color of the soil.

The water pressure heads at different points in the soil are measured directly with 20 tensiometers, each connected to its own transducer (Statham PM 131 TC) mounted on one of the perspex walls. The pressure ports are evenly distributed above and below the initial position of the water table. Another transducer measured the outflow volume, from the depth of water accumulated in a column connected to the right-hand side of the tank (Figure 1*b*).

Acquisition and Processing of the Data

Acquisition of the data is based on a cycling procedure defined by a series of two sequences: (1) the counting period of the gamma equipment, usually set at 60 s (during this interval the position of the measuring platforms is fixed) and (2) the scanning period, set at 40 s (during this period, all the scales and transducers are scanned, and the platforms are moved in order to reach their final positions before the initiation of the next counting period).

Every 100 s, the following series of data is obtained and punched on a teletype: (1) time from the beginning of the test, (2) location of the platform, (3) water content at three points $(x_1, z_1)(x_2, z_1)(x_2, z_2)$, each coordinate being determined by the locations of the platforms, (3) total outflow volume, and (4) soil water pressure for each one of the 20 tensiometers.

The data are processed by an IBM 1130 computer. Processing includes the systematic use of a plotter to follow rapidly the changes of θ or h at given points and to obtain at given times a map of water content and of hydraulic head (defined by $H = h - z$), using a numerical procedure of interpolations.

Determination of Soil Properties

Suction Curve

Because of the nature of the measuring technique, changes of water content and soil water pressure could not be measured at the same point. An interpolation technique was thus used to estimate from the experimental measurements of water pressure at different times, values appropriate to the points of measurement of water content. All of the pairs of values thus obtained were then plotted on the same graph, and a least squares regression used to define the moisture characteristic of the soil (Figure 2*b*) in terms of the analytical expression

$$\theta = \theta_s \frac{\alpha}{\alpha + |h|^\beta} \tag{1}$$

in which $\theta_S = 0.30$ cm^3/cm^3, $\alpha = 40.000$, and $\beta = 2.90$. There is significant scattering of the points about the mean values, but *Nielsen et al.* [1973] have indeed shown that the soil moisture characteristic is sensitive to even the smallest of local variations in density.

Hydraulic Conductivity

The water pressure–hydraulic conductivity relationship for our soil is given in Figure 2*c*. The experimental determination of the hydraulic conductivity was obtained directly from the analysis of several two-dimensional infiltration experiments. For such, the generalized form of Darcy's law gives

$$K(\theta) = \frac{|\langle q \rangle|}{|\langle \text{grad } H \rangle|} \tag{2}$$

where $|\langle q \rangle|$ is the modulus of the volumetric flux vector and $|\langle \text{grad } H \rangle|$ is the modulus of the gradient vector of hydraulic head at a particular point.

The calculation is much more complicated than for a one-dimensional experiment [*Vachaud and Thony*, 1971] because both the direction and the modulus of the water flux must be determined at each point of measurement. The following procedure was thus adopted.

Calculation of the fluxes. Considering an element of soil volume (Δx, Δz) surrounding a point $M(x, z)$ (see Figure 3) the modulus of the flux at that point is

$$|\bar{q}| = (q_x^2 + q_z^2)^{1/2} \tag{3}$$

where q_x and q_z are the horizontal and vertical flux components respectively. They can be as expressed as

$$q_x = \frac{q_x' + q_x''}{2} \qquad q_z = \frac{q_z' + q_z''}{2} \tag{4}$$

with q_x' and q_x'' the horizontal fluxes entering face AD and leaving face BC and q_z' and q_z'' the vertical fluxes entering face AB and leaving face CD.

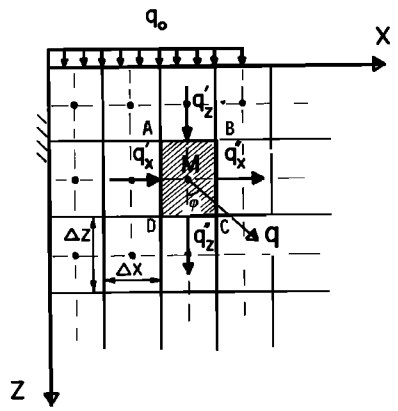

Fig. 3. Flux calculation grid.

The direction of the flux vector at point M is defined by

$$\tan \varphi = \frac{q_x}{q_z} \tag{5}$$

The different components of the flux vector were calculated for the element ABCD, using the continuity equation in the form

$$\frac{\Delta\theta}{\Delta t} = \frac{q_x' - q_x''}{\Delta x} + \frac{q_z' - q_z''}{\Delta z} \tag{6}$$

where $\Delta\theta/\Delta t$ represents the variation of the volumetric water content during the time interval Δt.

Combining (4), (5), and (6) gives

$$q_z'' = \frac{-\Delta\theta/\Delta t + 2q_x' - q_z'(\tan\varphi/\Delta x - 1/\Delta z)}{\tan\varphi/\Delta x + 1/\Delta z}$$
$$q_x'' = (q_z' + q_z'')\tan\varphi \tag{7}$$

Equations (3), (4), and (7) permit the calculation of the flux vector modulus at each point if q_x', q_z', $\Delta\theta/\Delta t$ and $\tan\varphi$ are known.

The value of φ can be obtained directly from a map of equipotential lines. In effect, the structure of the generalized Darcy's law means that, at each point, the vector $\vec{q}$ is orthogonal to the lines H = const. An automatic procedure was used to trace a family of curves H = const from the many measurements of water pressure obtained by the transducers at various points in the flow domain. Figure 4 illustrates such a tracing for t = 1 hr. The value of $\Delta\theta/\Delta t$ is obtained directly at the center of each element of the grid (the measurements point) from the instantaneous slope of the curves $\theta(t)$ measured by gammametry at different times (Figure 5).

Beginning the calculation at element 1 (Figure 4) where q_x' = 0 and $q_z' = q_0$ = 14.8 cm/hr, q_x'' and q_z'' can be found from (7), and therefore q_x, q_z, and $|\langle q\rangle|$ from (4) and (3), respectively. By this procedure, different instantaneous values of $|\vec{q}|$ at the center of each element can be determined step by step, since q_z'' leaving element 1 is also entering element 2 just as q_x'' enters element 6 (see Figure 4). The values of $|\langle q\rangle|$ are plotted against the measured values of water content at the center of each element, inferred at the same instant by interpolation from the curves in Figure 5.

It should be noted that the finite difference grid is chosen in such a way that the center of each element corresponds to a measurement point.

Calculation of $\langle grad\ H\rangle$. At each point $M(x, y)$ the value of $\langle \text{grad } H\rangle$ at a particular time t is obtained directly from the equipotential curves (Figure 4) with $|\langle \text{grad } H\rangle| = \partial H/\partial n$, where n is the normal distance between two equipotential lines surrounding point M.

Several infiltration runs were made with the flux q_0 varying from 2.5 to 35 cm/hr. For each trial the above calculation was made at different times. This allowed different $K(\theta)$ values to be obtained thus taking into account spatial variability. A change of variable, based on the $h(\theta)$ relationship given in

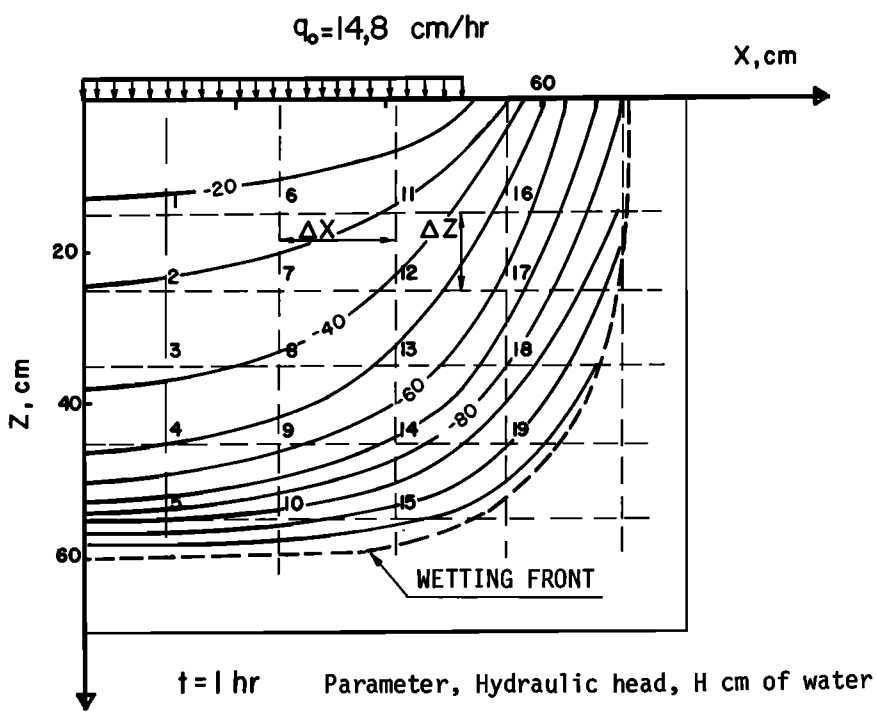

Fig. 4. Example of equipotential lines at time t = 1 hr.

Figure 2*b*, was finally used to obtain the $K(h)$ relationship of Figure 2*c*.

This procedure, though more complicated than using single dimensional flow, is preferable to destructive methods and to determinations made on reconstituted soil examples as was done by *Tang and Skaggs* [1977]. With that method, representativeness of measurement is not assured. Thus *Tang and Skaggs* [1977] suggest the possibility of an error in the determination of the hydraulic conductivity water content relationship to explain the relatively bad correlation between their calculated and measured results.

The hydraulic conductivity at saturation was obtained by applying Darcy's equation to a steady state flow between two trenches [*Vauclin*, 1975]. Under these conditions, the permeability at saturation K_s is given by the relationship

$$K_s = \frac{Q_s}{e(\eta + h_c)i} \tag{8}$$

where

- Q_s steady state flow rate measured at the outflow of the aquifer;
- e thickness of the slab of soil;
- η thickness of the aquifer at outflow measured relative to the substratum;
- h_c height of the capillary fringe;
- i slope of the free surface calculated at the outflow.

Flow in the capillary fringe has been shown by *Vauclin* [1975] to have some relevance to the estimating of the permeability at saturation. Therefore, unlike in the work of *Tang and Skaggs* [1977], one includes the capillary fringe as a part of the saturated zone.

The value obtained, $K_s = 35$ cm/hr, is for a practically horizontal flow. This was confirmed by a trial with vertical infiltration, in which the flux $q_0 = 35$ cm/hr gave a permanent gravity regime approaching natural saturation ($\theta = 0.30$). This validates the hypothesis of isotropy in relation to the porous media considered.

The continuous line on Figure 2*c* corresponds to a smoothing of the observed values by an analytical expression of the form

$$K = K_s \frac{A}{A + |h|^B} \tag{9}$$

where A and B are determined by the method of least squares.

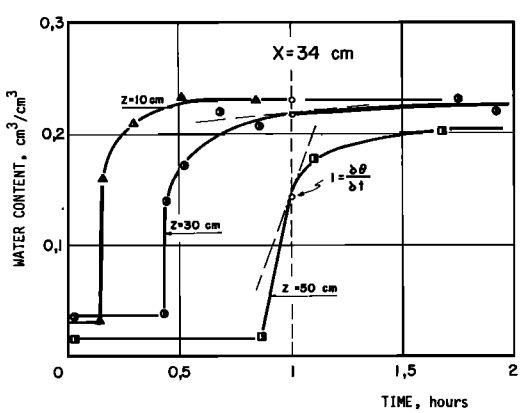

Fig. 5. Evolution of measured water content with time at the abscissa $X = 34$ cm for depths of 10, 30, and 50 cm.

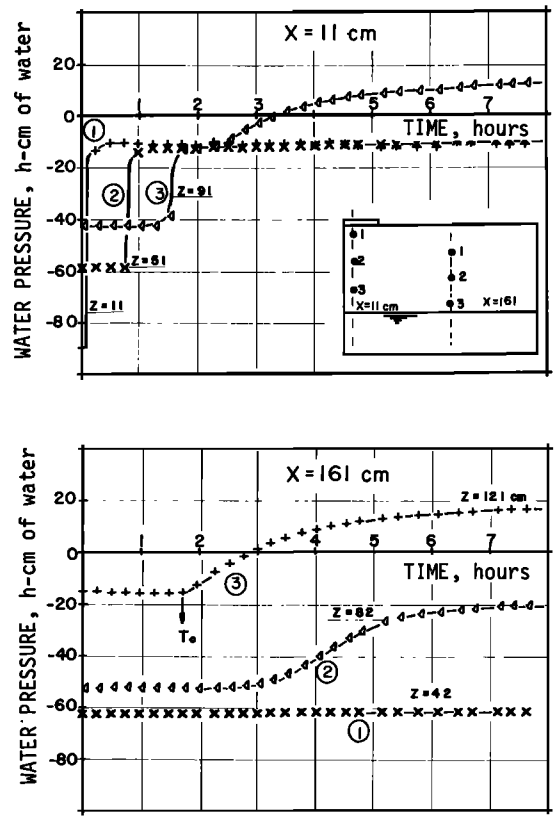

Fig. 6. Evolution of measured water pressure head with time at the abscissas $X = 11$ and 161 cm for different depths.

For the soil considered, it was found that $A = 2.99 \times 10^6$ and $B = 5.0$.

Experimental Results

Keeping in mind that the aims for obtaining experimental results were to obtain a good understanding of the physics of the flow and to test the validity of a numerical simulation model, we will present the results on two different scales: (1) a local study of water content and water pressure and (2) global results concerning the evolution of the water table and the total outflow.

Evolution of water pressure. As an example, Figure 6 shows the time-evolution of the water pressure obtained directly from the output of the transducers, at two abscissas: $x = 11$ cm, i.e., below the infiltration area, and $x = 161$ cm.

If we consider first the three transducers located at $x = 11$ cm, it is obvious that the flow is directed downward, the depth $z = 11$ cm being wetted before $z = 51$ cm and before $z = 91$ cm. The wetting is almost instantaneous, being characterized by a very sharp change of pressure head. Because, after wetting, the same pressure is obtained at all three depths, the flow has become gravitational. Finally, the water table reaches the point ($x = 11$, $z = 91$ cm) at $t = 3.2$ hr.

From the transducer outputs located at $x = 161$ cm, it is clear that the flow is upward, since $z = 121$ cm becomes wet before $z = 82$ cm. Water at the depth $z = 42$ cm remains at the same pressure throughout the experiment. Here the wetting is due to a rise in the water table, and the changes of water pressure are smooth. The water table reaches the point ($x = 161$, $z = 121$ cm) at $t = 2.9$ hr.

From similar measurements made at $x = 71$, 101, and 161 cm (where the other tensiometers were installed) we were able

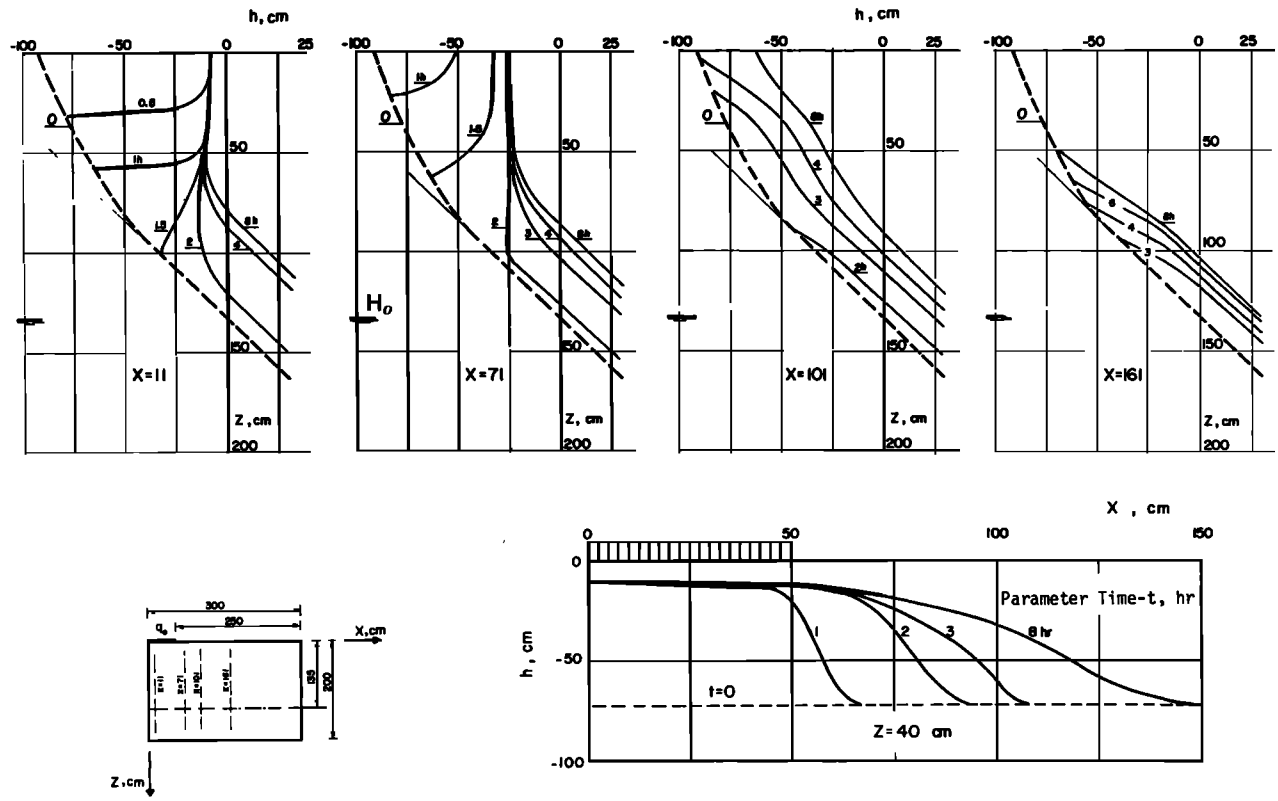

Fig. 7. Vertical and horizontal profiles of water pressure head, obtained experimentally at different times.

by a simple change of parameter to obtain the water pressure profiles shown in Figure 7. The upper part of this figure gives profiles of $h(z)$ at the several abscissas, and the profile at $t = 0$ corresponding to the initial values. The position of the water table ($h = 0$) at each abscissa at any given time can be easily obtained. The lower part of Figure 7 gives profiles of $h(x)$ at a given depth, viz., $z = 40$ cm. It shows clearly the lateral progression of the wetting zone.

Evolution of water content. Applying the same technique of analysis to the measurements of water content θ, Figure 8 gives measured profiles of $\theta(z)$ for different abscissas and different times. The profile corresponding to time $t = 0$ is the initial profile. It is thought that local heterogeneities in the packing of the material are responsible for the irregular shapes of these profiles.

Three sets of curves can be considered:

1. Below the infiltration zone ($x \leq 50$ cm) the flow is mostly vertically downward. The wetting front advances at a constant rate, and soon the water content near the surface reaches its maximum value ($\theta = 0.26$ cm^3/cm^3), this being controlled by the flux. Therefore $K(\theta = 0.26) = 14.8$ cm/hr. The water table is reached at about $t = 1.75$ hr. For $t > 2$ hr, changes of water content are minimal.

2. For $50 < x < 110$ cm, the flow component is mostly horizontal: wetting occurs by lateral flow, the water content increasing simultaneously at all depths for each value of x.

3. For $x \geq 110$ cm the flow is predominantly upward; no wetting occurs before $t = 1.75$ hr.

Global results. Figure 9 illustrates the evolution both of the infiltrated volume V_1, the outflow volume from the water table V_2, and the volume being stored in the soil V_3 (calculated from the water content profiles). For times $t < T_0 = 1.75$ hr there is no flow produced at the outflow of the aquifer. The infiltrated volume is entirely stored in the unsaturated zone. T_0 is defined as the transfer time. It should be noticed that a steady state is attained, for all practical purposes, by $t = 8$ hr, since the inflow and outflow curves then have the same slope.

In order to obtain water table profiles at given times, isovalues of the water pressures are mapped along with the 20 measurements obtained in the slab, and at each instant the line corresponding to $h = 0$ is defined as the free surface of the aquifer. The mounds obtained at 2, 3, 4, and 8 hr are shown in Figure 10. No change of pressure for the transducers located at $z = 135$ cm was detected for $t \leq 1.75$ hr.

NUMERICAL ANALYSIS

Numerical Schemes

For efficient use of computer time combined with high accuracy, the analysis was carried out in two stages:

For $t \leq T_0$. Flow occurs only in the unsaturated zone. Therefore the problem is described by the classical nonlinear parabolic equation:

$$C(h)\frac{\partial H}{\partial t} = \frac{\partial}{\partial x}\left(K(h)\frac{\partial H}{\partial x}\right) + \frac{\partial}{\partial z}\left(K(h)\frac{\partial H}{\partial z}\right) \tag{10}$$

where

- H hydraulic head given by $H = h - z$, cm of water;
- h soil water pressure, cm of water;
- $C(h)$ capillary capacity, equal to $d\theta/dh$, cm^{-1};
- $K(h)$ hydraulic conductivity, cm/hr;
- z is oriented positively downward.

Vauclin et al. [1979] showed that the transformation of (10) by the flux potential [*Rubin,* 1968] as defined by $U(h) = \int_{h_0}^{h} K(h)\,dh$ was advantageous in solving the infiltration equation in unsaturaged media. The discretization of the equation

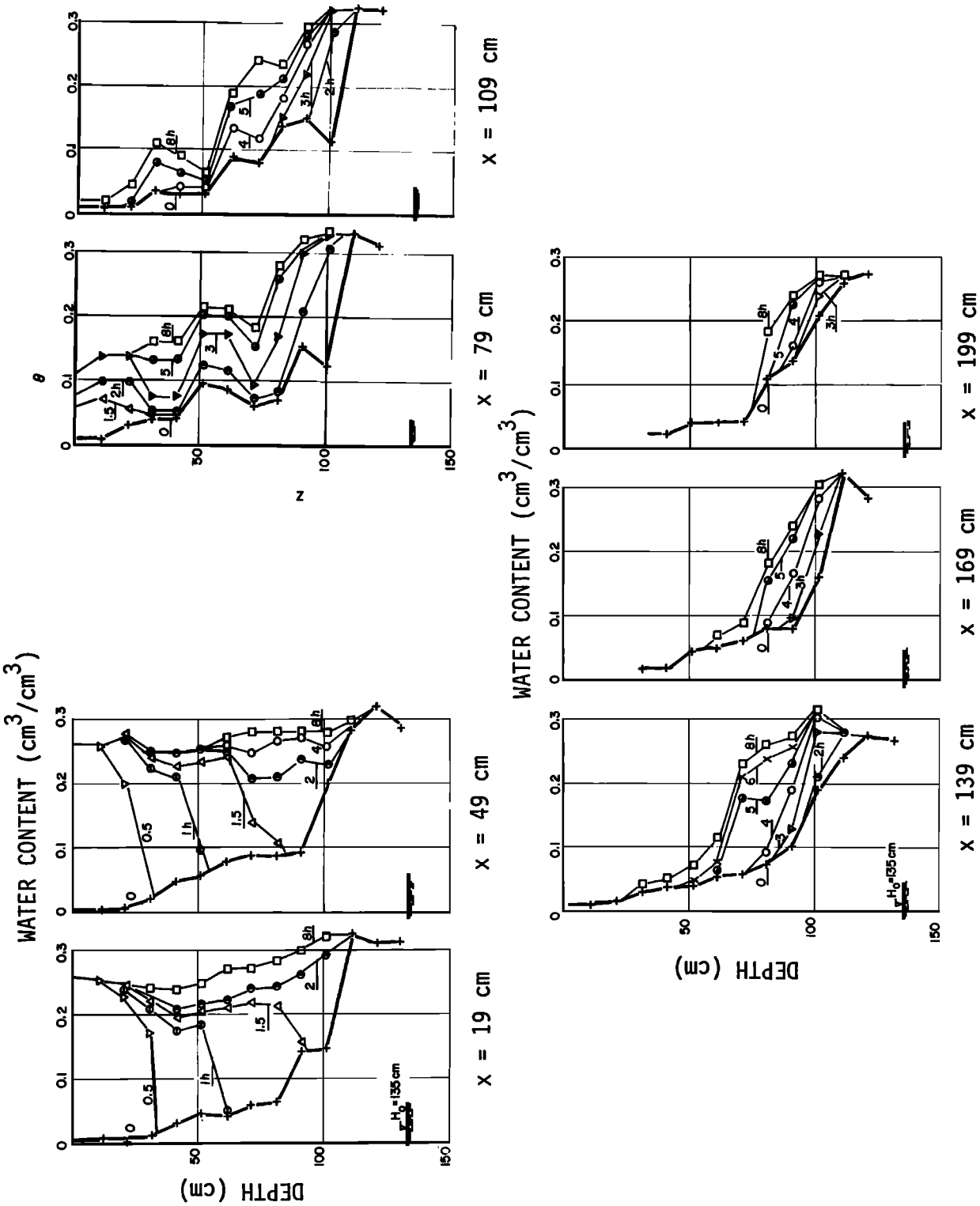

Fig. 8. Water content profiles measured at different abscissas for different times.

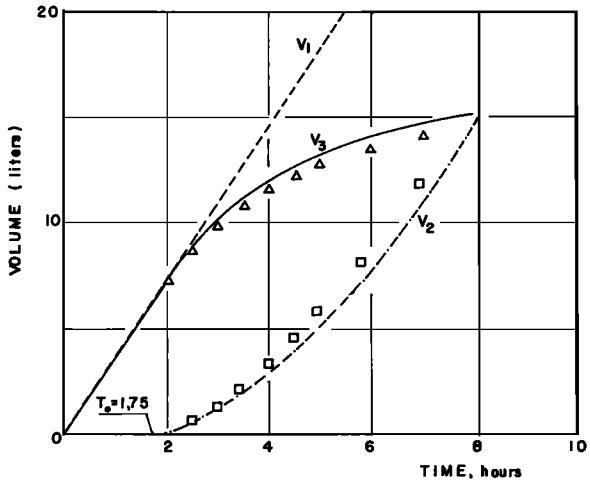

Fig. 9. Evolution of the volume of water entering (V_1), leaving (V_2), and stored within (V_3) the slab of soil during the recharge event. The symbols refer to experimental values. The curves for V_2 and V_3 were calculated with the scheme described in the numerical analysis section.

so transformed does not involve estimating the appropriate value of the coefficient K at the internodal calculation points where the solution is unknown. Additionally, because of its integral nature, variations in the U function are much slower than those in h. This reduces the numerical errors linked with the discretization.

Equation (10) is written in the form

$$F(U)\frac{\partial U}{\partial t} = \frac{\partial^2 U}{\partial x^2} + \frac{\partial^2 U}{\partial z^2} - G(U)\frac{\partial U}{\partial z} \qquad (11)$$

where

$$F(U) = \frac{1}{K}\frac{d\theta}{dh} \qquad G(U) = \frac{1}{K}\frac{dk}{dh}$$

The initial and boundary conditions are

$$z = 0 \qquad 0 < x \le L_0 \qquad \frac{\partial U}{\partial z} = K - q_0$$

(constant rate of infiltration)

$$z = 0 \qquad x > L_0 \qquad \frac{\partial U}{\partial z} = K$$

(no evaporation)

$$x = 0 \qquad 0 \le z \le Z(t) \qquad \frac{\partial U}{\partial x} = 0$$

(by symmetry)

$$x = X(t) \qquad 0 \le z \le Z(t) \qquad U = U_0(z)$$
$$z = Z(t) \qquad 0 \le x \le X(t) \qquad U = U_0(z)$$

(moving boundary) where $Z(t)$ and $X(t)$ are the coordinates of a point on the moving boundary represented by the wetting front, and $U_0(z)$ is the initial value of U at the depth considered.

Equation (11) has been solved directly with the use of the alternating direction and implicit (ADI) scheme [*Rubin*, 1968; *Remson*, 1971]. The grid dimension was chosen to be $\Delta x = \Delta z = 10$ cm for which a time step of 10 s guaranteed the stability of the numerical scheme.

For $t > T_o$. The flow occurs simultaneously in the unsaturated and saturated zones. Therefore a unique system should be considered, with boundary conditions applied to the geometric boundaries of the box.

It is known that (10) is valid for describing the flow in the unsaturated zone as well as in the saturated zone: however, in the saturated zone the equation degenerates because $C = 0$. Equation (10) becomes simply the Laplace equation. But at the same time, it changes from a nonlinear parabolic equation to a linear elliptic equation, and it is then necessary to use an iterative numerical scheme [*Peaceman and Rachford*, 1955; *Rubin*, 1968].

Consequently, during the second stage ($t > T_0$), (10) was applied to the entire slab of soil, with the following initial and boundary condition:

$$t = T_0 \qquad h^*(T_0, x, z) \qquad \theta^*(T_0, x, z)$$

which are known from the previous solution at $t = T_0$

$$t > T_0 \qquad z = 0 \qquad x \le L_0 \qquad -K\frac{\partial H}{\partial z} = q_0$$

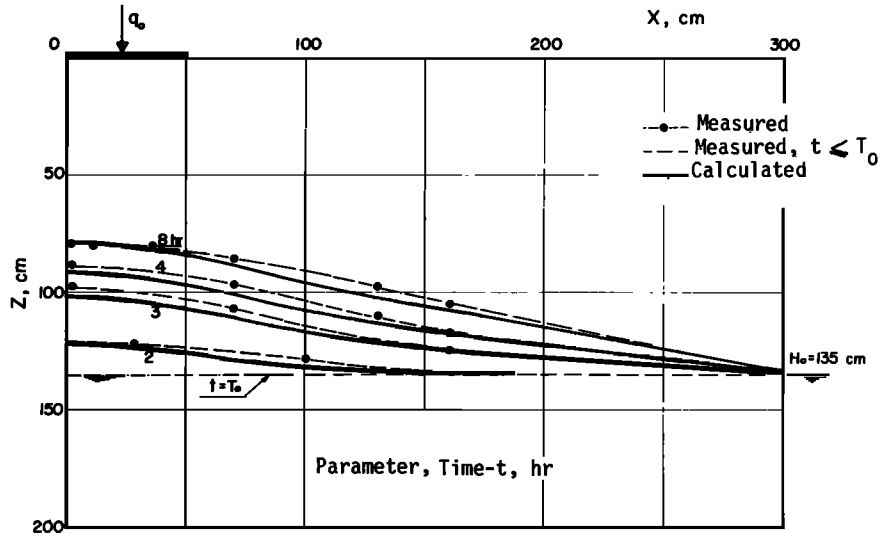

Fig. 10. Measured and calculated water table positions at different times.

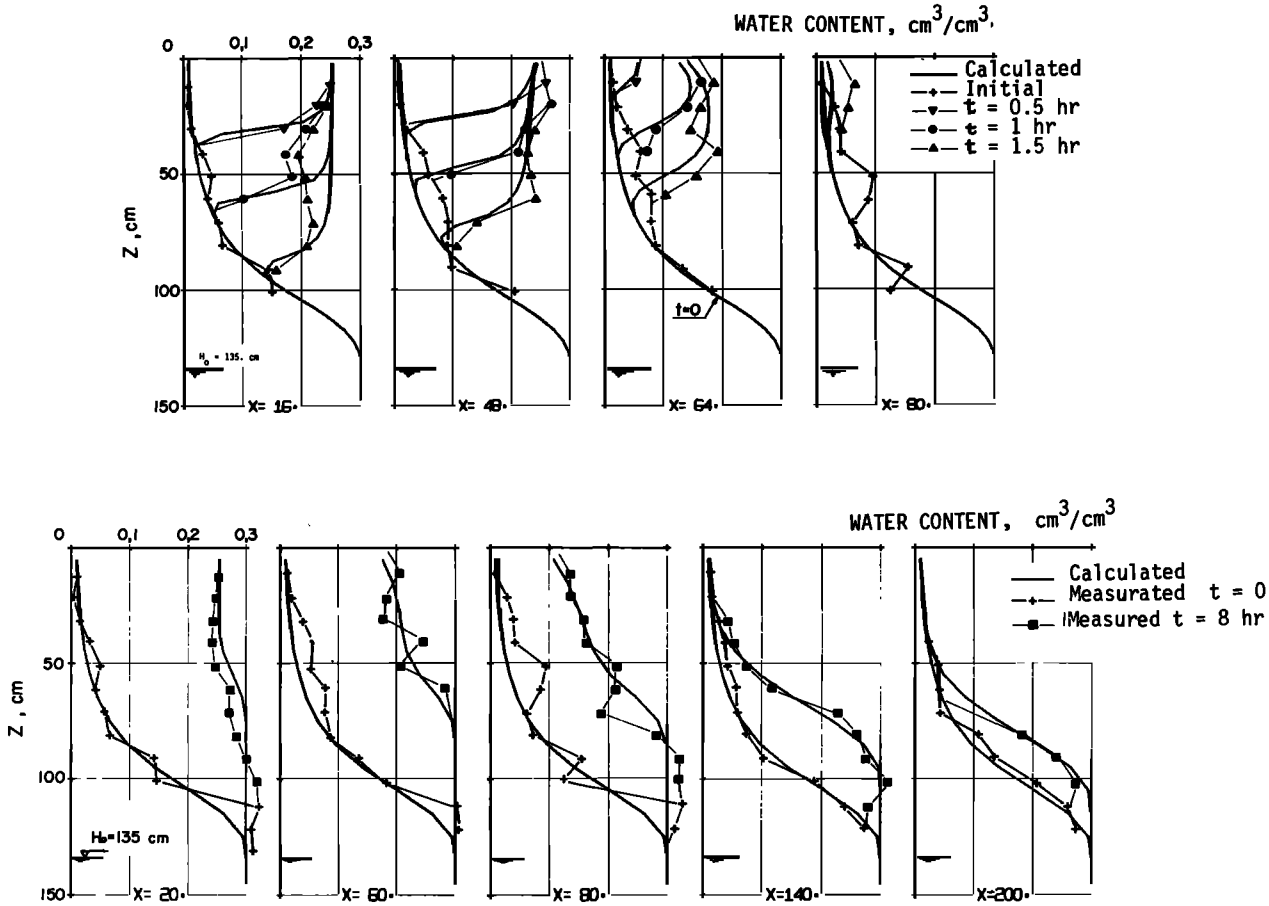

Fig. 11. Experimental and numerical water content profiles at different abscissas.

(constant rate of infiltration)

$$z = 0 \qquad x > L_0 \qquad \frac{\partial H}{\partial z} = 0$$

(no flux through the surface)

$$x = L \qquad z < z_s \qquad \frac{\partial H}{\partial x} = 0$$

(no horizontal flow)

$$x = L \qquad z_s \leq z \leq H_0 \qquad H = -z$$

(seepage surface)

$$x = L \qquad z \geq H_0 \qquad H = -H_0$$

(constant level in the ditch)

$$z = P \qquad \forall x \qquad \frac{\partial H}{\partial z} = 0$$

(impervious boundary)

$$x = 0 \qquad \forall z \qquad \frac{\partial H}{\partial x} = 0$$

(by symmetry) z_s is the depth of the seepage face, which has to be found by iteration [*Vauclin*, 1975].

To solve this second part of the problem, the ADIPIT method (with iterations) was used [*Rubin*, 1968; *Vauclin*, 1975]. In the discretization equations, a supplementary term was added to the left hand side of (10), to achieve a faster convergence of the iterative procedure. With the notations used by *Rubin* [1968] in his paper, the following values were chosen, namely, $R = 0.15$ and $S = 4$. For each time step, the cycles were repeated until the biggest difference between the hydraulic head values obtained in two successive iterations was smaller than 10^{-2} cm.

The space steps were the same as before. The time interval was defined as that required for the maximum flux of water (q_{max}) to move, in the soil, from one node to the next, i.e.,

$$\Delta t = 5 \times 10^{-3} \frac{\min(\Delta x, \Delta z)}{q_{max}}$$

Finally the internodal conductivities which appear in the discretized equations were calculated as geometric averages, since it had been proved [*Vauclin et al.*, 1979] that this method of weighting gives the most precise numerical solution (better than arithmetic of harmonic mean values applied to K or h).

At each time step, a test was performed on the value of h to decide if a node was in the unsaturated zone ($h < 0$) or in the saturated zone ($h \geq 0$). For a grid with 396 nodes the calculation time on an IBM 1130 computer was 3 min per time step.

Simulation of Local Variables

First the model was tested for its ability to simulate changes of local variables such as water content or the water pressure. As an example, Figure 11 compares experimental water content profiles obtained at given times, for given abscissas, with the corresponding numerical profiles. The numerical profiles

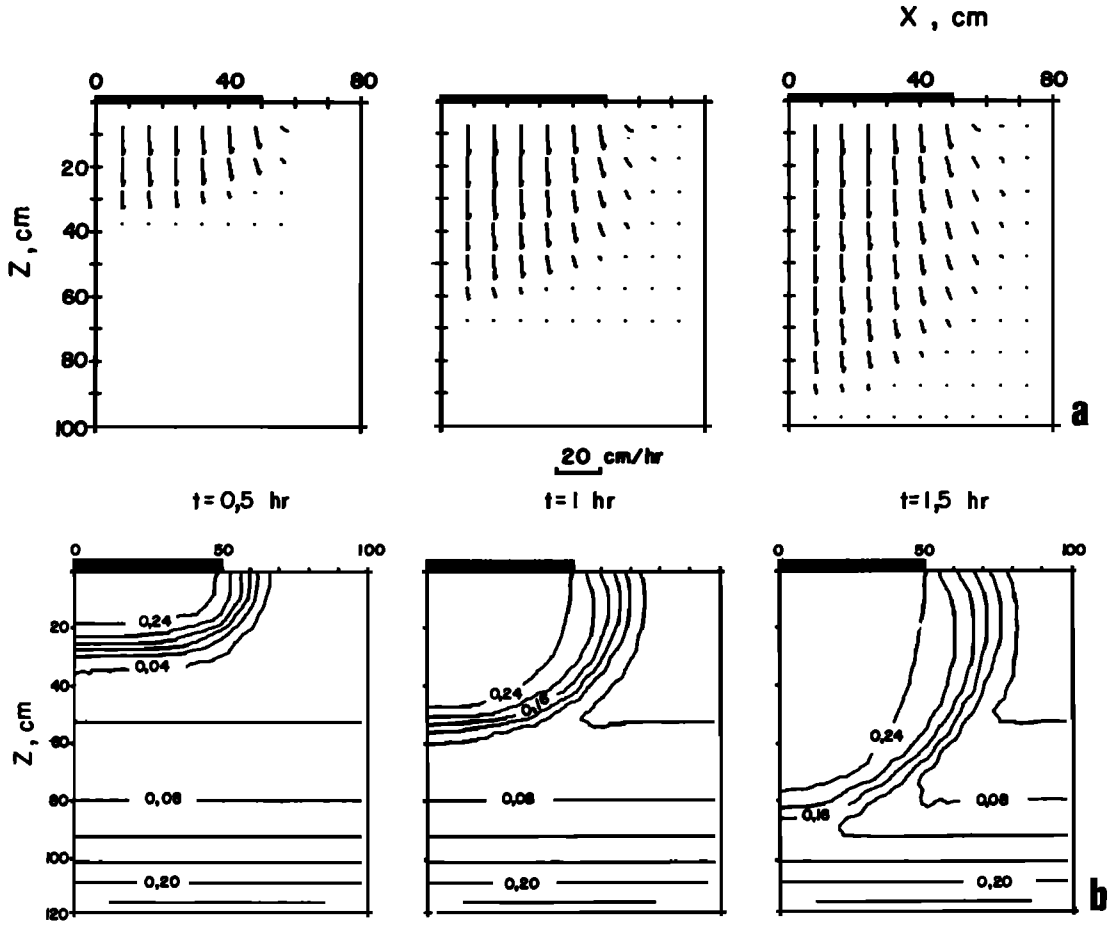

Fig. 12. Pattern of fluxes and contours of water content calculated at times $t = 0.5$, 1, and 1.5 hr after the start of infiltration.

are smoother, since the soil is assumed to be isotropic and homogeneous, but their shape and the advance of the wetting front are in excellent agreement with the measurements. Similar agreement was obtained with the water pressure profiles.

One benefit of the numerical method, once it is tested, is to give valuable information about some variables which are not directly accessible to measurement.

As an example, Figure 12 shows the pattern of flux at each calculation node on three occasions during the infiltration stage, as well as the corresponding contours of water content. In the upper part of the figure, the flux at each node is represented in a vectorial manner. The effect of lateral flow under the infiltration zone is clearly demonstrated.

Figure 13*a* shows a typical distribution of volumetric fluxes and the associated field of hydraulic head, at time $t = 3$ hr, or 1.25 hr after the initiation of the recharge. One can deduce that there is a significant flow across the free surface. For $x <$ 100 cm the flux passing across the free surface is directed downward, while for $x \geq 100$ cm the vertical component is directed upward. Thus the unsaturated zone is moistened by a rise in the level of the water table. The steady state regime (at $t = 8$ hr) (see Figure 13*b*) shows that values of the flux in the capillary fringe, limited by the line CF, are of the same order of magnitude as those below the free surface. This justifies using the formula (8) for calculating the permeability at saturation. In the two cases, experimental values have been quoted for the hydraulic head obtained at the tensiometer measurement points. Substantial agreement is found between experimentally and numerically obtained values, with the exception of the soil zone unaffected by the flow. This follows from the experimental profile not being completely hydrostatic, as shown by Figure 7, in conflict with the assumptions of the numerical simulation.

Simulation of Global Results

The growth of the water table mound after initiation of the recharge is well simulated, as shown by the curves in Figure 10.

The error in the prediction of the beginning of the growth is smaller than 0.5%. The small discrepancy between the experimental and the numerical profiles is due mostly to the vertical size of the grid used, which was $\Delta z = 10$ cm.

A comparison between experimental and numerical values of the outflow volume is given in Figure 9. The agreement again is very good.

Concept of Effective Infiltration

The numerical model permits us to introduce the concept of an effective infiltration being that which corresponds to the flow of water producing a particular rise of the free surface at a time t. Figure 14 gives, at times $t = 2$, 3, and 8 hr, the horizontal distribution of the vertical component of the flux $q_z(x)$ passing across a horizontal plane (B), situated close enough to the free surface for one to be able to assume that all the flow across the plane arrives at the free surface. The values of $q_z(x)$

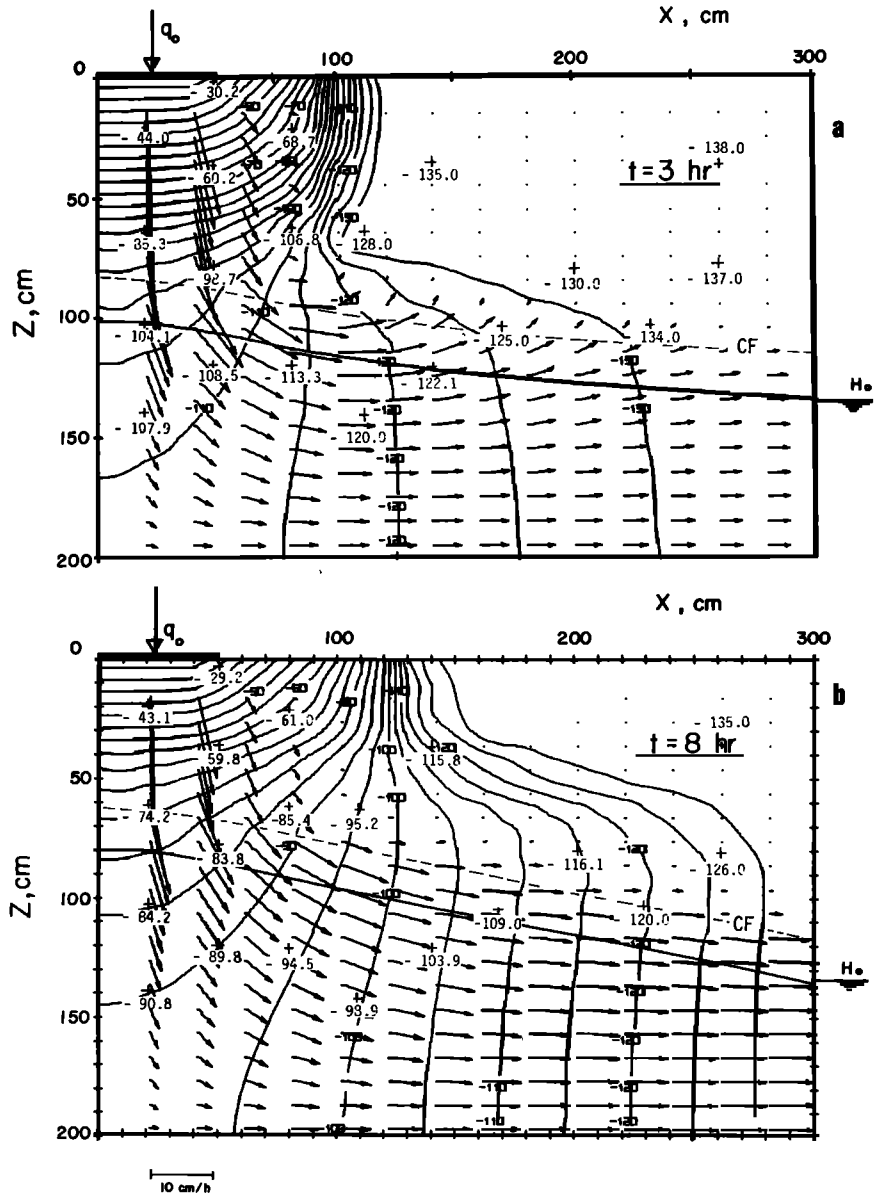

Fig. 13. Calculated distributions of flux and hydraulic head together with experimental values of the latter, represented by the numbers with crosses, and expressed in centimeters of water for (*a*) $t = 3$ hr and (*b*) $t = 8$ hr.

are obtained by using the numerical model. The area

$$A_1 = \int_0^L q_z(x)\,dx$$

gives the flow rate arriving at the free surface for unit thickness of soil. The area A_2 represents the unit flow infiltrated across the soil surface (A). Table 1 gives the relationship between the flow arriving at the free surface and that imposed at the soil surface.

It appears from the data that the flow applied at the soil surface over a width L_0 reaches the aquifer over a significantly wider zone, but with of course a weaker intensity. It is not until 8 hr have passed that the ratio λ approaches 1.

Conclusions and Discussion

This study shows that it is not possible to neglect the transfer of water through the unsaturated zone in predicting the recharge of a water table aquifer. From a practical point of view the most important items to know are the time of transfer and the volume reaching the aquifer at a given time.

Most of the classical approaches to this problem (*Polubarinova-Kochina* [1962], *Hantush* [1967], *Glover* [1961], *Marino* [1967], and others) have been based on the assumptions that (1) the transfer is instantaneous, (2) at any time the distribution of flux reaching the aquifer is equal to the distribution of flux applied at the soil surface, and (3) above the water table the soil has a uniform water content, equal to the so-called 'residual' water content.

The rise of the water table during a time interval Δt is then simply

$$\Delta z = \frac{q_0 \Delta t}{m} \tag{12}$$

where m is the effective porosity. The work described here has shown that these assumptions have no physical basis at all.

To emphasize the inability of those three assumptions (deal-

TABLE 1. Time Evolution of the Ratio λ Between the Rate A_1 (per Unit Thickness of Soil) at Which Water Reaches the Free Surface of the Water Table Located at z_B and that (A_2) Imposed at the Soil Surface

t_h	1.75	2	3	8
z_B, cm	135	115	95	75
A_1, cm²/hr	0	270	534	736
A_2, cm²/hr	740	740	740	740
$\lambda = A_1/A_2$	0.	0.36	0.72	0.99

ing with what we call the 'saturated approach') to model the problem considered in this article, they have been tested in three different ways: the viscous flow analog model of Hele Shaw, the numerical solution of Boussinesq's equation, and the approach developed by *Hantush* [1967] for predicting the rise in water table at $x = 0$. Recall that only the first model satisfies strictly the three basic assumptions. A detailed analysis of the results is given by *Vachaud et al.* [1975], we will consider here only two illustrations.

Figure 15*a* shows the evolution of the piezometric levels at $x = 0$ and $x = 200$ cm obtained with the different saturated approaches compared with the curves actually determined from the sand box. Owing to the relatively small curvature of the free surface, there are no significant differences between the three classical solutions in this case. The comparison between the volumes being stored under the saturated zone is given in Figure 15*b*.

The following points appear clearly. First, the classical saturated approach cannot predict the duration of the time of transfer, which is an important unknown in any problem of recharge. Second, if we translate arbitrarily to the right the curves obtained by the Hele Shaw model, in order to match the beginning of the recharge with the true time of arrival of the infiltration front, the solution obtained with the classical

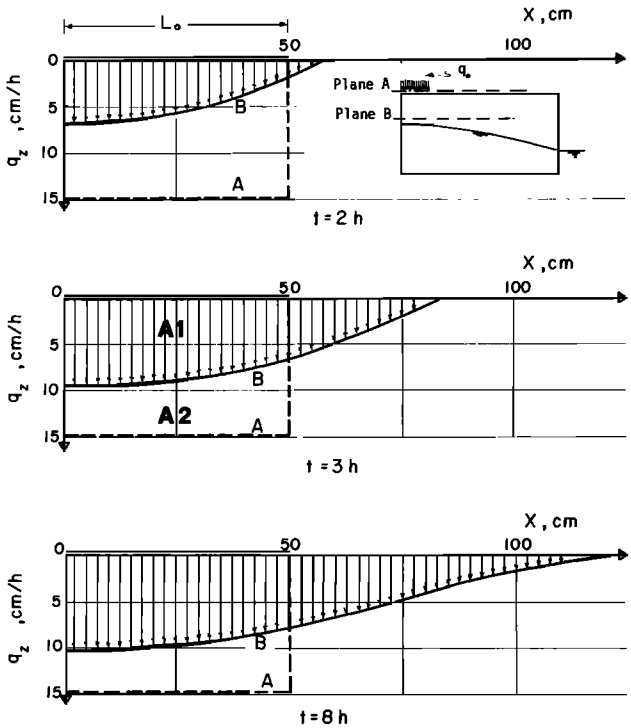

Fig. 14. Distribution of the vertical component of the fluxes passing through the soil surface (plane A) and arriving at the water table (plane B).

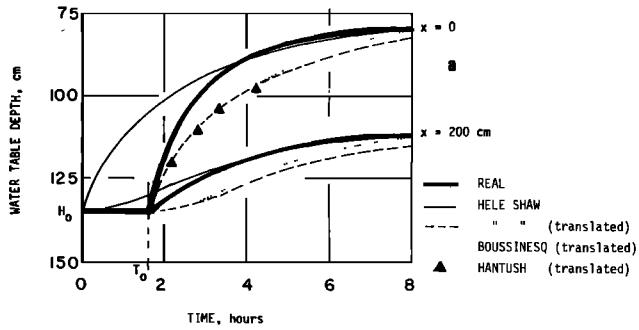

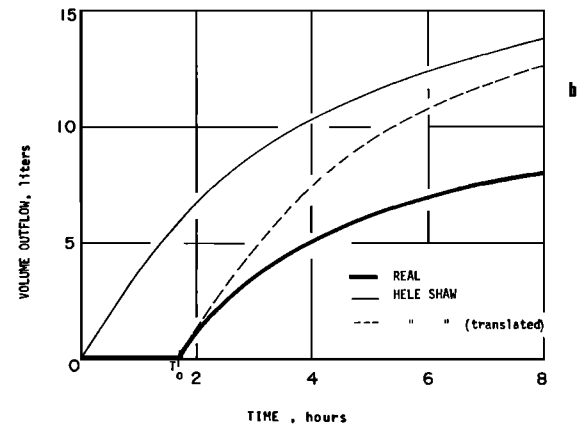

Fig. 15. (*a*) Comparison of the measured rates of change of water table depth at two abscissas (0 and 200 cm) with those predicted by various saturated models. The 'translated' curves refer to the classical models operated as from the time of transfer T_0, supposedly known. (*b*) Comparison of outflow volumes measured in the sand box with those obtained by the Hele Shaw analog, with and without translation.

approach corresponds systematically to an underestimation of the rise of the water table and an overestimation of the volume stored beneath it.

The apparent contradiction here simply illustrates that no simple correlation exists in practice between a rise in level of the free surface (change of water pressure) and the increase of volume under the free surface. Depending upon the shape of the suction curve, a fairly large change of water pressure (near $h = 0$) can indeed yield a very small change of water storage. This fact is completely neglected in the classical saturated approach (see (12)).

Due to the nonlinearity of the problem, it is not possible to use a series of nomographs to predict, for a given soil the time of transfer as a function of the initial depth of the water table and of the boundary condition being applied at the soil surface. Solutions cannot be superposed, as can be done in a linear system. In illustration of our model's ability to predict other situations, Figure 16 shows curves giving time of transfer as a function of flux q_0, or of initial depth of water table H_0. Each point on the curve is the result of a separate complete experiment, similar to the one described here, but for different initial and boundary conditions. The details are given by *Khanji* [1975].

In conclusion it appears that one ought to consider a unified numerical treatment of unsaturated-saturated flow to solve correctly the problem of transient recharge of a water

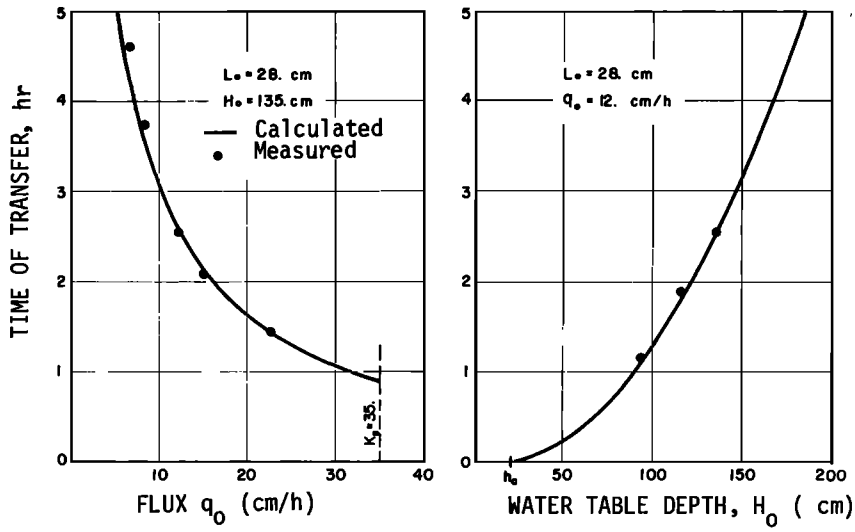

Fig. 16. Calculated and measured times of transfer as functions of volumetric flux and water table depth.

table aquifer. The validity of the numerical approach proposed in this study has been well illustrated. The influence of the unsaturated zone may have been exaggerated by the geometry of the sand box model, but nevertheless it appears that the classical saturated approach is totally unable to determine the transfer time for water in the unsaturated zone. The model which has been developed permits us to predict the evolution with time of the shape of the wetting front in the unsaturated zone, the volume of water reaching the water table, and the rise in the groundwater mound provided the initial and boundary conditions are known, together with curves of $K(h)$ and $h(\theta)$.

Acknowledgments. This work was partly supported by Délégation Générale à la Recherche Scientifique et Technique (Paris) and by Centre National de la Recherche Scientifique (Paris).

REFERENCES

Cooley, R. L., A finite difference method for unsteady flow in variably saturated porous media, Application to a single pumping well, *Water Resour. Res.*, *7*(6), 1607–1625, 1971.

Freeze, R. A., Three dimensional transient saturated-unsaturated flow in a groundwater basin, *Water Resour. Res.*, *7*(2), 347–366, 1971.

Glover, R. E., Mathematical derivations as pertain to groundwater recharge, report, 81 pp., U.S. Dep. of Agr., Agr. Res. Serv., Fort Collins, Colo., 1961.

Hantush, N. S., Growth and decay of groundwater mounds in response to uniform percolation, *Water Resour. Res.*, *3*(1), 227–234, 1967.

Khanji, D., Etude de la recharge de nappes à surface libre par infiltration, Ph.D. thesis, 252 pp., Univ. Sci. et Méd. de Grenoble, Grenoble, France, 1975.

Marino, M. A., Hele-Shaw model study of the growth and decay of groundwater ridges, *J. Geophys. Res.*, *72*(4), 1195–1205, 1967.

Narasimham, T. N., A unified numerical model for saturated-unsaturated groundwater flow, Ph.D. thesis, Univ. of Calif., Berkeley, 1975.

Narasimham, T. N., and P. A. Witherspoon, Numerical model for saturated-unsaturated flow in deformable porous media, 3, Applications, *Water Resour. Res.*, *14*, 1017–1034, 1978.

Nielsen, D. R., J. W. Biggar, and K. T. Erh, Spatial variability of field measured soil water properties, *Hilgardia*, *42*, 215–260, 1973.

Peaceman, D. W., and H. H. Rachford, The numerical solution of parabolic and elliptic differential equations, *J. Soc. Ind. Appl. Math.*, *3*, 24–41, 1955.

Polubarinova-Kochina, P. Y., *Theory of Groundwater Movement*, translated by J. M. R. De Wiest, 613 pp., Princeton University Press, Princeton, N. J., 1962.

Remson, I., G. M. Hornberger, and F. D. Molz, *Numerical Methods in Subsurface Hydrology*, 389 pp., John Wiley, New York, 1971.

Rubin, J., Theoretical analysis of two-dimensional, transient flow of water in unsaturated and partly unsaturated soils, *Soil Sci. Soc. Amer. Proc.*, *32*(5), 607–615, 1968.

Tang, Y. K., and R. W. Skaggs, Experimental evaluation of theoretical solutions for subsurface drainage and irrigation, *Water Resour. Res.*, *13*(6), 957–965, 1977.

Vachaud, G., and J. L. Thony, Hysteresis during infiltration and redistribution in a soil column at different initial water contents, *Water Resour. Res.*, *7*, 111–127, 1971.

Vachaud, G., M. Vauclin, and D. Khanji, Etude expérimentale des transferts bidimensionnels dans la zone non saturée, *Houille Blanche*, *1*, 65–74, 1973.

Vachaud, G., M. Vauclin, and R. Haverkamp, Towards a comprehensive simulation of transient water table flow problems in modeling, in *Computer Simulation of Water Resources Systems*, edited by G. C. Vansteenkiste, pp. 103–119, North-Holland, Amsterdam, 1975.

Vauclin, M., Etude expérimentale et numérique du drainage de nappes à surface libre, Influence de la zone non saturée, Ph.D. thesis, 196 pp., Univ. Sci. et Méd. de Grenoble, Grenoble, France, 1975.

Vauclin, M., R. Haverkamp, and G. Vachaud, *Etude de la Résolution Numérique de l'Équation d'Eau en Milieu Nosaturé*, 165 pp., Presses Universitaires de Grenoble, 1979.

(Received November 20, 1978;
revised March 26, 1979;
accepted April 17, 1979.)